Supplementary Materials for

Anomalously low electrostatic bending stiffness of graphene oxide 2D membranes regulates its environmental fate in aquatic ecosystems

Mohamad Ali Sanjari Shahrezaei [1,2†], S. Mohammad-Reza Taheri [3†], Hesam Nikfazan [4,5], Alexandra Satalov[1,6], Mohsen Moazzami Gudarzi [7*], Seyed Hamed Aboutalebi [1,3*]

[1] Pasargad Institute for Advanced Innovative Solutions (PIAIS), 1991633361, Tehran, Iran

[2] JETCO, Advanced Automotive Technologies Research Center, Tehran, 1389814611, Iran

[3] Condensed Matter National Laboratory, Institute for Research in Fundamental Sciences (IPM), Tehran, 19395-5531, Iran

[4] GrapheneX, Tehran, 1541938564, Iran

[5] Tadbirgran Kimia Pishtaz, Tehran, 1541938564, Iran

[6] Leibniz University Hannover, Institute for Inorganic Chemistry, Hannover, Germany

[7] National Graphene Institute; University of Manchester, Manchester, United Kingdom

† These authors contribute equally to this work.

*Correspondence to: mohsen.moazzamigudarzi@manchester.ac.uk, sha942@uowmail.edu.au

This PDF file includes:

Supplementary Text section1 to section 4

Table S1

Figs. S1 to S7

Supplementary Text

S1. Analysing the aggregation and charging behaviour of GO:

The electrophoresis data were extracted from five different references. (Figure 3 of [1], Figure 2C of [2], Figure 2 of [3],Figure S7 of [4], Figures 2a and S4 of [5], and Figures 1 and S3 of [6] [except for NaCl data which is based on the publication of the same authors in [7]). The data at low ionic strength were not taken into account due to the fact that the surface charge density is lower at this regimen because of the shift in acid-base equilibrium, [8] and/or ion condensation. [9,10]

In some cases, the electrophoretic mobility (μ) data were converted to zeta potential (ζ) using the Smoluchowski equation:

$$\zeta = \frac{\eta}{\varepsilon\varepsilon_0}\mu \qquad (1)$$

Where ε, ε_0 and η are dielectric constant of water, vacuum permittivity and viscosity of water, respectively.

In order to calculate the surface potential, one needs to have information about the position of the slipping plane relative to the surface. In addition, it is required to know how the electric potential decays from the surface in this region in order to estimate the surface potential from the zeta potential data. To the best of our knowledge, there is no unified theory to do so and the behaviour of the interfaces depends on different factors such as the types of ions and interfaces. [11] We, however, simplified the problem by assuming the electric potential decays as it is predicted by the Poisson-Boltzmann theory and assumed that the slipping plane is located at a fixed distance of 0.7 nm (d_{Stern}) away from the interface irrespective of types of ions and ionic strength. It should be noted that this estimation for slipping plane thickness matches with previous approximations for the thickness of the Stern layer. [9,12,13] [14] To this end, the surface potentials (ψ_0) were derived from the zeta potential using the following equation. [15]

$$\psi_0 = \frac{4k_BT}{ze}\tan^{-1}\left[\exp(\kappa.d_{Stern})\tan\left(\frac{ze\xi}{4k_BT}\right)\right] \qquad (2)$$

Where $e$is the elementary charge, z is the valence of counterions, k_B is the Bolzmann constant, T is the absolute temperature, and κ^{-1} is the Debye length which is defined as follows:

$$\kappa^{-1} = \left(\frac{k_BT\varepsilon\varepsilon_0}{2e^2I}\right)^{\frac{1}{2}} \qquad (3)$$

I stands for ionic strength and is given by the relation:

$$I = \frac{1}{2}\sum_i z_i^2 c_i \quad (4)$$

Where z_i is the valence of ions and c_i is the concentration of the corresponding ions.

The resulting surface potential data can now be used to find the effective surface charge density of graphene oxide (GO). These two quantities are related through the following equation: [16]

$$\sigma = -\left\{2k_B T \varepsilon \varepsilon_0 \sum_i c_i \left[\exp\left(-\frac{z_i e \psi_0}{k_B T}\right) - 1\right]\right\}^{\frac{1}{2}} \quad (5)$$

Please note that the negative sign in the pre-factor states the fact that GO sheets are negatively charged.

The extracted data are presented in Table S1.

S2. Derivation of general form of Schultz-Hardy rule:

We started with the assumption that the interaction between particles is the sum of vdW and electrical double layer forces:

$$W_{total} = W_{vdW} + W_{EDL} \quad (6)$$

It is known that vdW forces between different objects follow a power-law behaviour:

$$W_{vdW} = -\frac{C}{d^m} \quad (7)$$

The negative sign is a result of the attractive nature of these forces between similar particles. The factor C controls the magnitude of the force and it is directly related to Hamaker constant. The power factor m depends on the dimensionality of the particles.

We model the double layer forces using a linearized form of Poisson-Boltzmann theory:

$$W_{EDL} = \frac{2\sigma^2}{\varepsilon\varepsilon_0\kappa}\exp(-\kappa d) \quad (8)$$

In order for particles to aggregates without any barrier, the following conditions should therefore satisfy:

$$W_{total} = 0 \quad (9)$$

$$\frac{\partial}{\partial d}W_{total} = 0 \quad (10)$$

The above equations lead to:

$$W_{total} = \frac{2\sigma^2}{\varepsilon\varepsilon_0\kappa}\exp(-\kappa d) - \frac{C}{d^m} = 0 \quad (11)$$

$$\frac{\partial}{\partial d}W_{total} = -\frac{2\sigma^2}{\varepsilon\varepsilon_0}\exp(-\kappa d) + \frac{mC}{d^{m+1}} = 0 \quad (12)$$

Solving these two equations, one can find the position of energy barrier, d_{max} , as:

$$d_{max} = m \cdot \kappa^{-1} \quad (13)$$

Inserting this distance to the equation (6) gives:

$$\kappa^{m+1} = \frac{2m^m\exp(-m)}{\varepsilon\varepsilon_0}\sigma^2 \quad (14)$$

Given that by definition:

$$\kappa \approx I^{\frac{1}{2}} \quad (15)$$

We arrive to the following relation:

$$I_{critical} = CCIS \sim \sigma^{\frac{4}{m+1}} \quad (16)$$

One can approximate the surface potential using the following relation [17]:

$$\sigma = \varepsilon\varepsilon_0\kappa\psi_0 \quad (17)$$

Given that for a $z{:}z$ electrolyte the effective surface potential can be approximated as follows:

$$\psi_{eff} = \frac{4k_BT}{ze}\tan\left(\frac{ze\psi_0}{4k_BT}\right) \quad (18)$$

For highly charged surfaces, the effective potential saturates at a limiting value:

$$\psi_{eff} \rightarrow \frac{4k_BT}{ze} \quad (19)$$

Thus, one can arrive to:

$$CCIS \sim \psi_0^{\frac{4}{m-1}} \quad (20)$$

For highly charged surfaces in $z{:}z$ electrolytes this leads to:

$$CCIS \sim z^{-\frac{4}{m-1}} \quad (21)$$

The ionic strength in $z{:}z$ electrolytes scales with the valence of salt as:

$$I \sim z^{-2} \quad (22)$$

Therefore, the critical coagulation concentration will have a following relation with valence:

$$CCC \sim z^{-\left(\frac{4}{m-1}+2\right)} \quad (23)$$

For spherical particles, $m = 2$ and the celebrated Schultz-Hardy rule ($CCC \sim z^{-6}$) is recovered. For ideal 2D particles $m = 4$ and:

$$CCC \sim z^{-\frac{10}{3}} \quad (24)$$

S3. DLVO and xDLVO calculations:

Interaction energy between GO layers was modelled using DLVO theory for thin nanosheets.[18] As discussed above:

$$I_{critical} = CCIS \sim \sigma^{\frac{4}{m+1}} \quad (25)$$

DLVO theory predicts $m \approx 3.6$ for GO (assuming thickness of about 0.7 nm. Note that when thickness approach zero, then $m \to 4$). In Figure 5 of the main text, we argued that the experimental data from literature follows this power law when the surface charge density of GO is relatively high (roughly above 1 mC/m^2). At low surface charge density, assuming that aggregation starts when the energy barrier is merely few kT the predicted CCC can change significantly. Therefore, we re-evaluated the DLVO theory prediction by changing the equation (4) to:

$$W_{total} = kT \quad (26)$$

In order to know the interaction energy, one needs to know the interacting area among GO sheets. Here, we assumed that GO sheets are disk with a diameter of 500 nm (close to hydrodynamic radius of GO reported in most of the 6 references reviewed here). Given that the effective overlapping area of two disks colliding randomly is $\frac{1}{2\pi}A$ (A is the disks' area), then it is possible to find CCC for the case where the energy barrier is one kT. GO is then modelled as a disk with thickness of 0.7 nm and refractive index of 1.85. Then CCC was calculated for different surface charge density according to[18]. To compare the calculated CCC with the experimental data, the surface charge density in the presence of NaCl (the highest among the salts reviewed here) is assumed to be 25 mC/m^2.

S4. Environmental Exposure Pathways:

In order to simplify the simulations and calculations, an equivalent sphere technique is generally used in order to model graphene oxide. This is the case as sphere is the only shape whose size can be described by one unique number. Using one unique number to describe our particle liberates us from using three or even more numbers to define our particles, which although more accurate is inconvenient for modelling, simulation and calculations purposes. This practice is generally called the equivalent sphere theory. Depending on the properties, we then calculate different sizes based on equivalent sphere theory. As an example, if it is the surface area that is important, as usually is the case when chemical reactions or particles' activity are of importance, one usually considers either number-surface mean, D [2.0], or surface area moment mean, D [3,2], which is also known as Sauter mean diameter. On the other hand, if it is the mass or volume which is important, either number-weight mean, D [3,0], or weight moment mean, D [4,3], which is also known as De Brouckere mean diameter, are considered.

Techniques such as dynamic light scattering (DLS) or Laser particle size analysis, which are unequivocally used as the basis for particle sizing also calculate distribution based around volume which is in effect the same as D [4,3]. So, the question is whether the assumptions regarding effective radius are valid and what role, if any, they play on environmental exposure pathways. To further delve into this question, we should remind ourselves of the following points;

1. Since DLS essentially measures fluctuations in scattered light intensity due to diffusing particles, it can only calculate the hydrodynamic radius of a spherical particle or at least a 3D particle through the Stokes–Einstein equation and not the real dimension.
2. The hydrodynamic diameter of a non-spherical particle is the diameter of a sphere that has the same translational diffusion speed as the particle. If the shape of a particle changes in a way that affects the diffusion speed, then the hydrodynamic size will change. For example, small changes in the length of a rod-shaped particle will directly affect the size, whereas changes in the rod's diameter, which will hardly affect the diffusion speed, will be difficult to detect.

So, one serious implication is that treating GO as a hypothetical hard sphere described by one single number affects the hydrodynamic radius and translational diffusion. Diffusion coefficient is usually calculated by fitting correlation curve to an exponential function. The as-calculated diffusion function will then be used to calculate frictional coefficient;

$$D = \frac{kT}{f} \tag{27}$$

Whereas D is the diffusion coefficient, f is the frictional coefficient, k is the Boltzmann constant, and T is the temperature.

Given that the inherent assumption in the calculation of the diffusion coefficient is that the particles are hard spheres that diffuse with the same speed as our particles, we can see that the frictional coefficient will be greatly affected.

Considering that the surface chemistry of graphene oxide is much more complicated than the models presented in literature possessing many functional groups that have strong interactions with the solvent (e.g. water), we therefore suggest a more sophisticated model should be developed to encompass all these factors. Nevertheless, we propose graphene oxide (and other nanomaterials) will go through the route presented in Figure S1. when being transported from freshwater into an estuary and then to the marine environment.

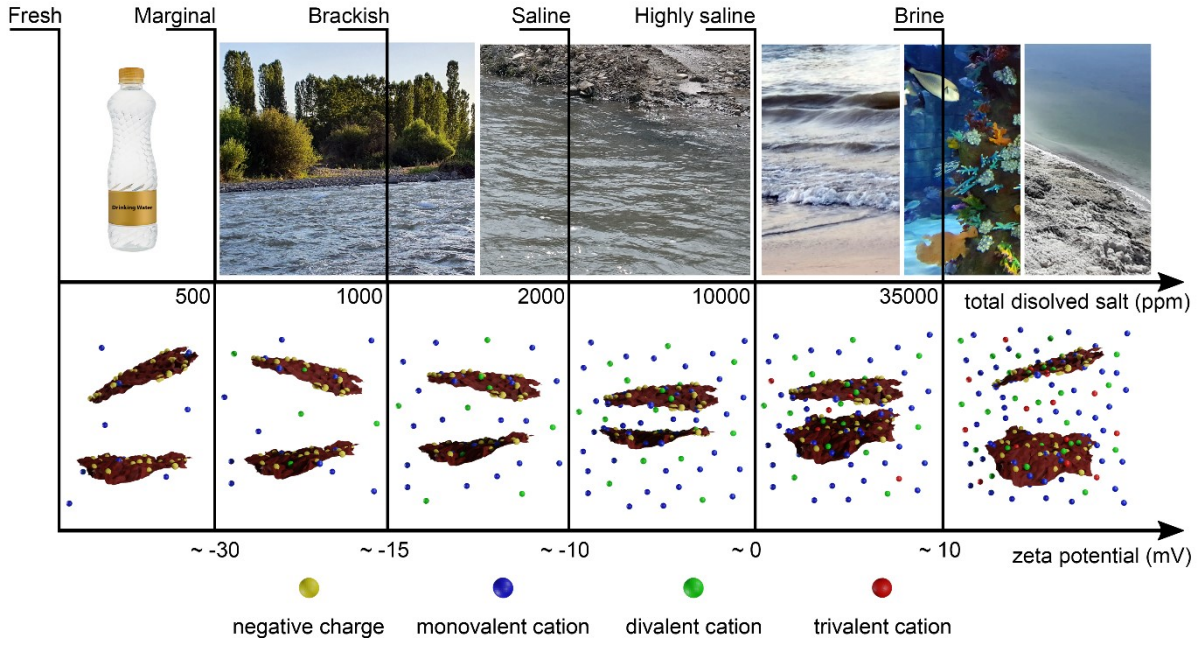

Fig. S1. **Environmental exposure pathways.** In fresh water, where the concentration of total dissolved salts is less than 500 ppm, graphene oxide sheets remain stable as the zeta potential is typically less than -30 mV. This is the direct result of the prevalence of the repulsive electric double layer forces in between GO sheets. However, travelling further into brackish and then saline water, where the concentration of metallic cations increases, attractive vdW forces become dominant and graphene oxide sheets tend to aggregate. At higher concentration of metallic monovalent and divalent cations (highly saline water), the cations can be specifically adsorbed on the surface of GO neutralizing the negative surface charge leading to fast aggregation of GO sheets in highly saline water. At this concentration range, the aggregation can outweigh any other effects resulting in the precipitation of GO sheets, consequently leading to less activity compared to the normal non-aggregated state. However, going further into marine and seawater environment, where the concentration of the salts is typically above 35000 ppm,

the surface charge profile of GO sheets becomes predominantly positive and charge reversal happens. It should be noted that a positive surface charge has been categorically associated with a higher risk of nanoparticle (NP) toxicity.[19] Therefore, we propose that GO sheets at this concentration range where the zeta potential value is also positive can become even more dangerous to aquatic life.

Table S1. The data used in Figure 5 is presented in here.

Salt type	Salt concentration (M)	Zeta potential (mV)	Surface Potential (mV)	Surface Charge Density (C/m^2)	CCIS (M) Average SCD (C/m^2)
Data is calculated from ref [3].					
NaCl	**0.08**	**-23.94**	**-49.69**	**-0.03721**	0.036
	0.06	-24.84	-46.65	-0.02974	
	0.04	-31.27	-53.16	-0.02875	-0.0272±0.0034
	0.02	-39.65	-58.55	-0.0232	
	0.01	-45.26	-59.99	-0.01697	
AgCl	**0.08**	**-10.53**	**-20.88**	**-0.01381**	0.019
	0.06	-13.09	-23.76	-0.01373	
	0.04	-16.97	-27.74	-0.01325	-0.0131±0.0004
	0.02	-27.55	-39.54	-0.01402	
	0.01	-35.17	-45.77	-0.01185	
	0.008	-39.45	-50.21	-0.01193	
KCl	**0.08**	**-14.19**	**-28.38**	**-0.01921**	0.028
	0.06	-19.66	-36.26	-0.02193	
	0.04	-22.29	-36.86	-0.01825	-0.0174±0.0013
	0.02	-32.60	-47.27	-0.01745	
	0.01	-40.83	-53.66	-0.01456	
	0.008	-42.22	-53.97	-0.01312	
$MgCl_2$	**0.001**	**-22.55**	**-26.22**	**-0.00303**	0.0045
	0.0009	-22.91	-26.46	-0.0029	
	0.0008	-23.78	-27.27	-0.00282	-0.00262±0.00013
	0.0007	-24.51	-27.89	-0.0027	
	0.0006	-24.74	-27.88	-0.0025	
	0.0005	-25.15	-28.07	-0.00229	
	0.0004	-25.93	-28.62	-0.00209	

$CaCl_2$	**0.001**	**-21.05**	**-24.41**	**-0.00282**	0.00405
	0.0009	-21.60	-24.88	-0.00272	
	0.00085	-21.05	-24.13	-0.00257	
	0.0008	-21.10	-24.08	-0.00249	-0.00243±0.00010
	0.0007	-21.01	-23.77	-0.0023	
	0.0006	-23.15	-26.03	-0.00233	
	0.0005	-24.19	-26.96	-0.0022	
	0.0004	-25.02	-27.59	-0.00202	
$CdCl_2$	**0.001**	**-19.73**	**-22.83**	**-0.00264**	0.0039
	0.0009	-19.96	-22.93	-0.00251	
	0.0008	-21.28	-24.30	-0.00251	
	0.0007	-22.05	-24.99	-0.00241	-0.00227±0.00011
	0.0006	-22.56	-25.34	-0.00227	
	0.0005	-22.83	-25.40	-0.00207	
	0.0004	-24.24	-26.71	-0.00195	
	0.0003	-25.57	-27.84	-0.00176	
$CuCl_2$	**0.001**	**-14.86**	**-17.08**	**-0.00199**	0.002175
	0.0009	-15.91	-18.18	-0.002	
	0.0008	-17.55	-19.93	-0.00206	
	0.0007	-18.55	-20.92	-0.00202	-0.00192±0.00005
	0.0006	-19.19	-21.47	-0.00192	
	0.0005	-19.24	-21.31	-0.00174	
	0.0004	-21.11	-23.17	-0.00169	
$PbCl_2$	**0.001**	**-5.45**	**-6.22**	**-0.00075**	0.0009
	0.0009	-9.55	-10.84	-0.00122	
	0.0008	-8.00	-9.01	-0.00096	
	0.0007	-11.73	-13.14	-0.00129	-0.00108±0.000062
	0.0006	-11.28	-12.52	-0.00114	
	0.0005	-12.19	-13.42	-0.00111	
	0.0004	-15.10	-16.49	-0.00121	
	0.0003	-14.38	-15.51	-0.00099	
$CrCl_3$	**7.00E-05**	**-14.04**	**-14.83**	**-0.00062**	0.00051
	6.00E-05	-16.91	-17.84	-0.00068	
	5.00E-05	-18.41	-19.35	-0.00067	
	4.00E-05	-21.03	-22.05	-0.00067	-0.0007±0.000025
	3.00E-05	-24.03	-25.11	-0.00066	

	2.00E-05	-33.71	-35.36	-0.00075	
	1.00E-05	-48.51	-51.42	-0.00082	
Data is calculated from ref [14].					
NaCl	**0.2**	**-11.49**	**-34.46**	**-0.03776**	0.188
	0.18	-12.71	-36.20	-0.03792	
	0.15	-16.85	-44.65	-0.0445	-0.0432±0.0023
	0.12	-21.52	-52.59	-0.04909	
	0.1	-23.82	-54.26	-0.04673	
$MgCl_2$	**0.008**	**-3.87**	**-5.61**	**-0.00192**	0.0117
	0.0045	-4.33	-5.72	-0.00146	
	0.0036	-4.56	-5.85	-0.00134	-0.00162±0.00016
	0.003	-4.98	-6.25	-0.0013	
	0.0026	-8.73	-10.83	-0.00206	
$CaCl_2$	**0.005**	**-3.94**	**-5.29**	**-0.00143**	0.0078
	0.003	-3.94	-4.95	-0.00104	
	0.0025	-4.63	-5.70	-0.00109	-0.00131±0.00011
	0.0019	-7.47	-8.97	-0.00147	
	0.0013	-9.88	-11.51	-0.00155	
Data is calculated from ref [1].					
NaCl	**0.1**	**-23.46**	**-53.32**	**-0.04565**	0.044
	0.08	-24.43	-50.84	-0.03833	
	0.05	-30.49	-55.26	-0.03386	-0.0392±0.0024
	0.03	-43.73	-72.34	-0.03892	
$MgCl_2$	**0.001**	**-22.45**	**-26.10**	**-0.00301**	0.0039
	0.0005	-25.01	-27.91	-0.00228	
	0.0001	-27.70	-29.12	-0.00107	-0.00177±0.00053
	5.00E-05	-27.40	-28.38	-0.00073	
$CaCl_2$	**0.001**	**-20.14**	**-23.33**	**-0.00269**	0.0027
	0.0005	-23.76	-26.46	-0.00216	
	0.0001	-24.63	-25.84	-0.00094	-0.00164±0.00047
	5.00E-05	-28.10	-29.12	-0.00075	
Data is calculated from ref [4].					

NaCl	**0.02**	**-26.57**	**-38.07**	**-0.01341**	0.11
	0.04	-24.97	-41.58	-0.02106	
	0.05	-22.86	-40.28	-0.02266	
	0.08	-22.78	-47.01	-0.03466	-0.0312±0.0040
	0.1	-19.46	-43.24	-0.03493	
	0.105	-18.18	-41.00	-0.03356	
	0.16	-14.89	-40.32	-0.04059	
	0.2	-14.00	-42.71	-0.04866	
$CaCl_2$	**0.0002**	**-18.15**	**-19.35**	**-0.001**	0.00798
	0.00025	-17.85	-19.17	-0.00111	
	0.0003	-17.29	-18.68	-0.00119	
	0.00075	-15.31	-17.27	-0.00174	
	0.001	-14.21	-16.32	-0.0019	-0.00213±0.00028
	0.0014	-13.91	-16.38	-0.00226	
	0.0018	-14.27	-17.19	-0.00268	
	0.0023	-14.09	-17.39	-0.00306	
	0.0026	-14.09	-17.63	-0.0033	
	0.0025	-13.53	-16.83	-0.0031	
Data is calculated from [5,6]					
NaCl	**0.0375**	**-35.17**	**-59.62**	**-0.03258**	0.19
	0.05	-27.20	-48.63	-0.02861	-0.0470±0.0060
	0.075	-25.56	-52.17	-0.0384	
	0.1	-23.95	-54.61	-0.04713	
	0.12	-21.5	-52.54	-0.04903	
	0.14	-21.43	-56.66	-0.05864	
	0.175	-20.74	-62.05	-0.07452	
$MgCl_2$	**0.0033**	**-15.40**	**-19.90**	**-0.00418**	0.01623
	0.0005	-20.43	-22.65	-0.00185	-0.00351±0.00041
	0.00075	-20.12	-22.84	-0.00228	
	0.001	-18.90	-21.84	-0.00252	
	0.0015	-17.68	-21.07	-0.00298	
	0.002	-17.20	-21.05	-0.00344	
	0.003	-15.78	-20.16	-0.00404	
	0.004	-15.09	-19.99	-0.00463	
	0.006	-14.09	-19.87	-0.00563	

$CaCl_2$	**0.00025**	**-20.30**	**-21.83**	**-0.00126**	0.00483
	0.0005	-17.79	-19.68	-0.00161	-0.00204±0.00031
	0.00083	-16.98	-19.32	-0.00204	
	0.001	-16.52	-19.02	-0.00221	
	0.002	-15.50	-18.90	-0.0031	
Data is Calculated from[7]					
NaCl	**0.01**	**-32.5**	**-42.14**	**-0.0107**	0.03
	0.03	-30	-47.14	-0.0213	-0.02375±0.00554
	0.05	-25	-44.34	-0.02548	
	0.1	-20.5	-45.81	-0.03752	
CsCl	**0.012**	**-32.8**	**-43.64**	**-0.01224**	0.0212
	0.014	-32.6	-44.4	-0.0135	-0.01433±0.000552
	0.016	-31.9	-44.36	-0.01442	
	0.018	-29.9	-42.28	-0.01442	
	0.02	-29.6	-42.65	-0.01536	
	0.024	-27.6	-41.05	-0.01606	
$Sr(NO_3)_2$	**0.0001**	**-20.2**	**-21.15**	**-0.00077**	0.0018
	0.0002	-19.6	-20.91	-0.00108	
	0.0003	-16.3	-17.60	-0.00112	
	0.0004	-15.6	-17.04	-0.00125	-0.00138±0.000102
	0.0005	-15.2	-16.77	-0.00138	
	0.0006	-14.5	-16.14	-0.00146	
	0.0007	-14.9	-16.74	-0.00163	
	0.0008	-14.5	-16.41	-0.00171	
	0.0009	-13.3	-15.15	-0.00168	
	0.001	-13.1	-15.03	-0.00175	
$UO_2(NO_3)_2$	**0.0001**	**-18.8**	**-19.67**	**-0.00072**	0.00111
	0.0002	-12.3	-13.07	-0.00069	-0.000963±0.000057
	0.0003	-12.5	-13.47	-0.00086	
	0.0004	-12	-13.08	-0.00097	
	0.0005	-11.1	-12.21	-0.00102	
	0.0006	-10.4	-11.54	-0.00105	
	0.0007	-9.7	-10.85	-0.00107	
	0.0008	-9.8	-11.05	-0.00117	
	0.0009	-8.75	-9.93	-0.00112	

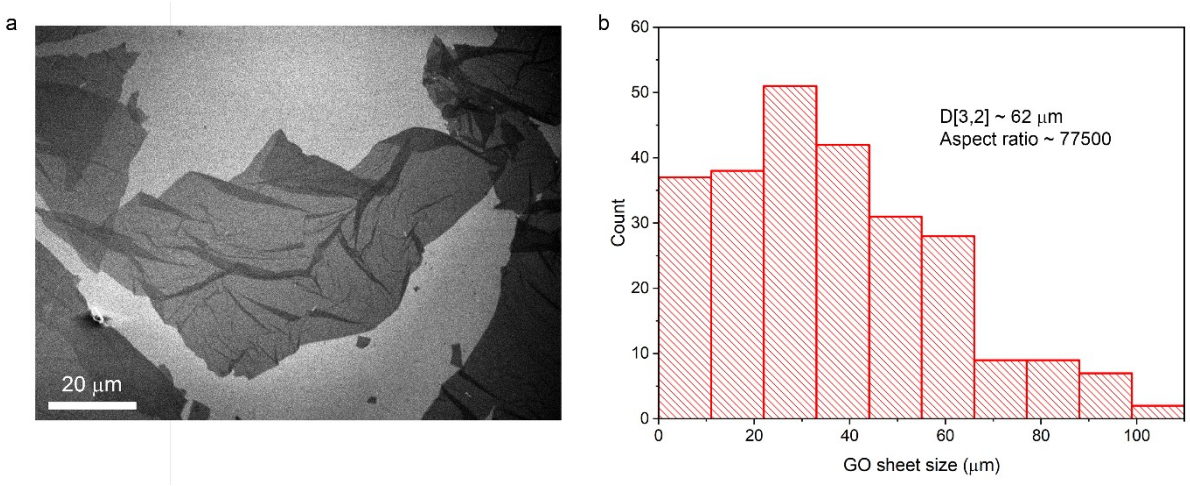

Fig. S2. **Size distribution and representative scanning electron micrograph of GO sheets.** The size of more than 200 individual GO sheets was measured to calculate the aspect ratio. a) Representative SEM image of GO sheets in our as-prepared GO dispersions representative of the wrinkled structure of GO. The wrinkled morphology is associated with thermal undulations which is known to affect the strength of GO sheets and shown to reduce the effective rigidity, just like fluid layers.[20,21] b) The corresponding distribution of GO sheet sizes and the as calculated aspect ratio based on D[3,2] of these samples.

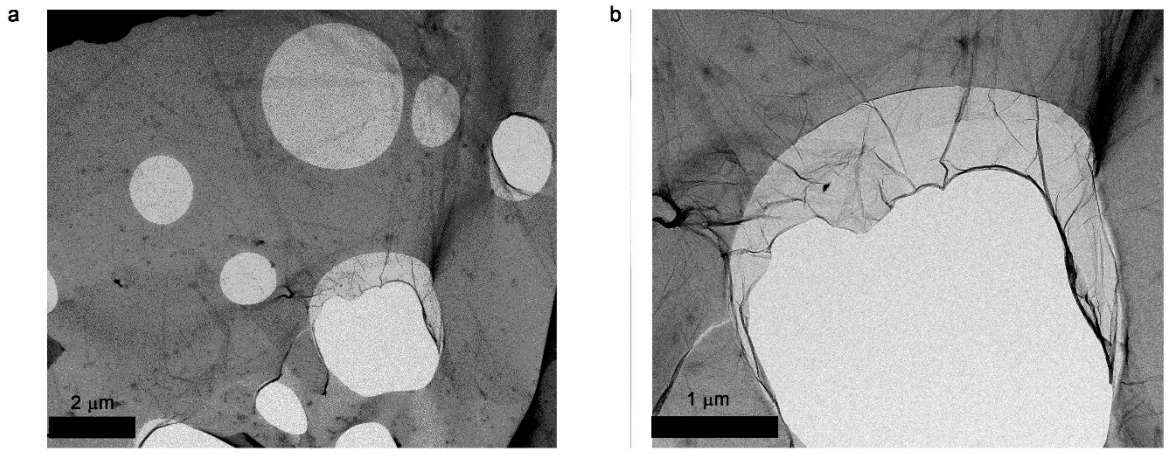

Fig. S3. **Representative transmission electron micrograph of GO sheets.** The wrinkled morphology is associated with thermal undulations which is known to affect the strength of GO sheets and shown to reduce the effective rigidity, just like fluid layers.

Fig. S4. **Polarized optical micrograph of GO dispersion.** The gigantic aspect ratio of our as-prepared amphiphilic GO sheets facilitate the formation of liquid crystals at concentrations as low as 0.1 g/L.

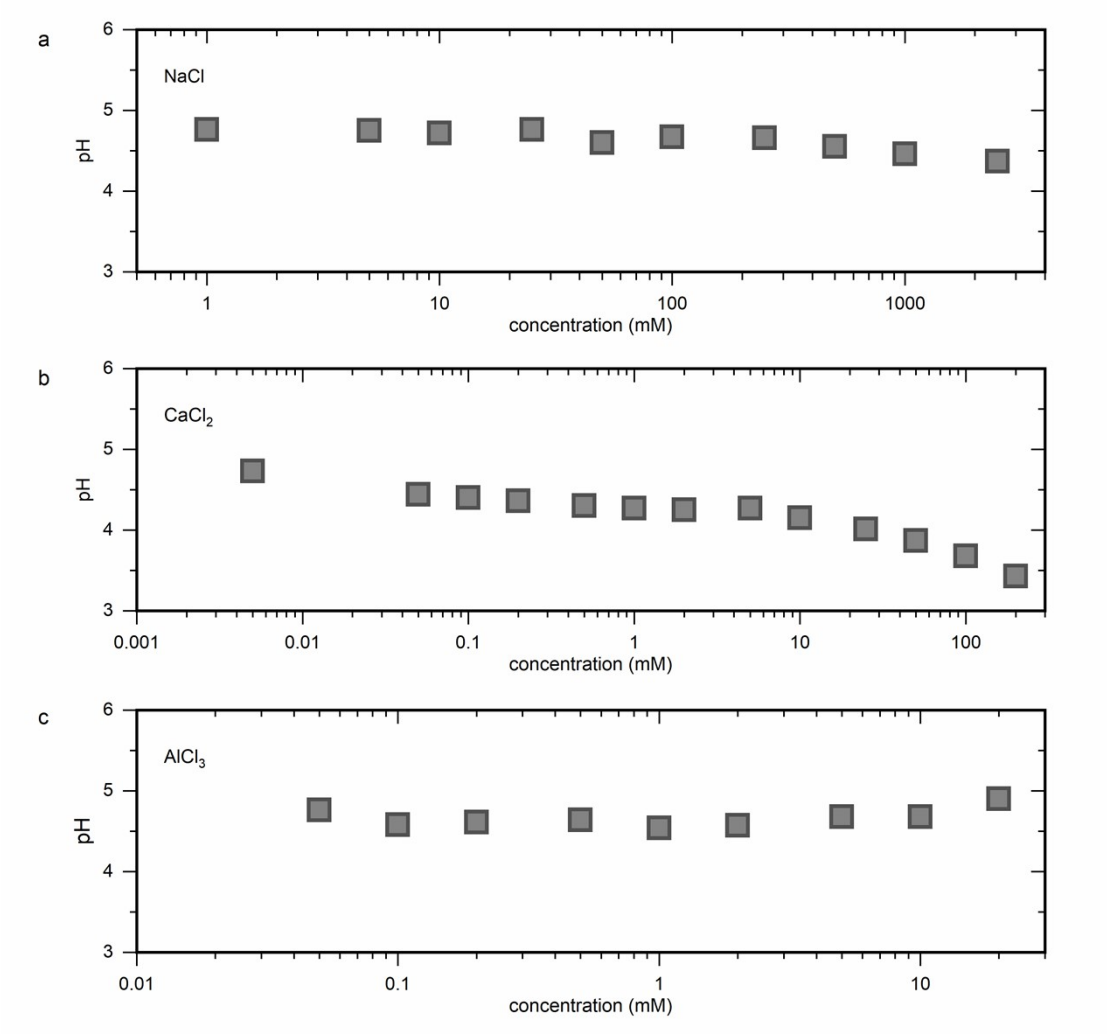

Fig. S5. **pH value vs. salt concentration.** As depicted, the pH range falls between 3-5 for all concentrations of a) NaCl, b) $CaCl_2$ and c) $AlCl_3$. The insets signify the low concentration region of original graphs.

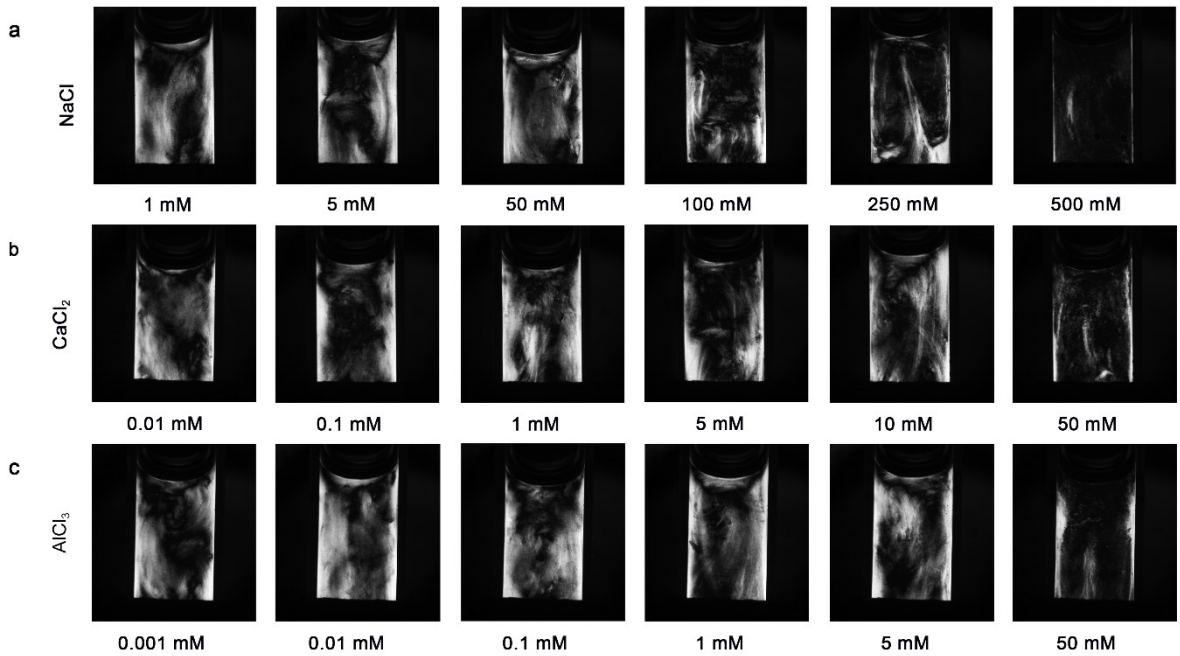

Fig. S6. **Using the optical setup presented in d, we determined the liquid crystallinity of our as-prepared GO dispersions (0.25 g/L) in the presence of metallic cations.** The polarized optical micrographs presented in e-g) unambiguously reveal the nematic liquid crystal phase further verifying the flat structure of GO sheets at all salt concentrations. This indicates the minor role of electrostatic contribution in the rigidity of GO. The disappearance of the liquid crystalline texture at very high salt concentrations, is due to the breakdown of colloidal stability of the GO particles. [18] After a critical concentration of salt, the repulsive double layer forces become so short-ranged that the vdW forces overcome the repulsive forces and the GO particles aggregates. The aggregation of GO sheets will decrease the effective aspect ratio of the particles due to stacking of the GO sheets, which essentially leads to nematic to isotropic transition.

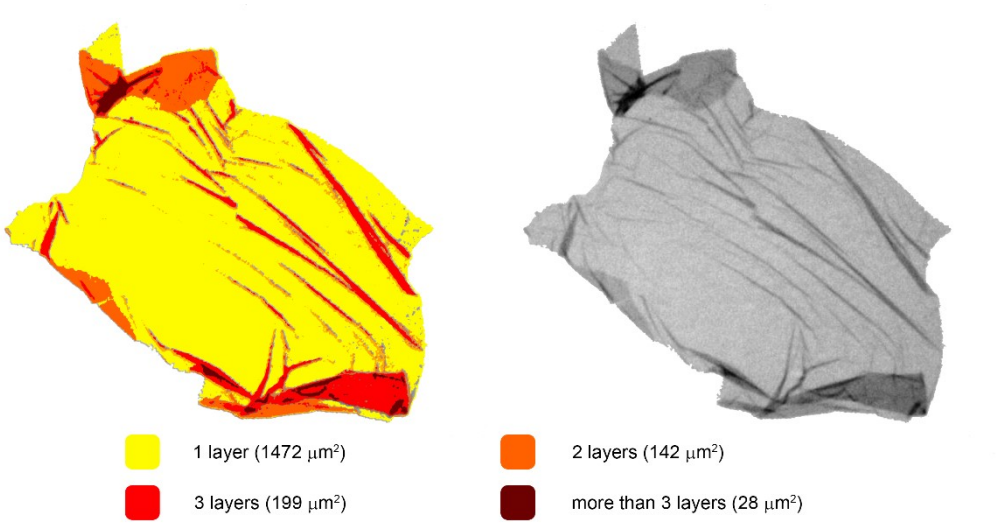

Fig. S7. One can calculate the apparent aspect ratio (the ratio of apparent lateral size to the thickness) is close to the fully stretched form of GO.

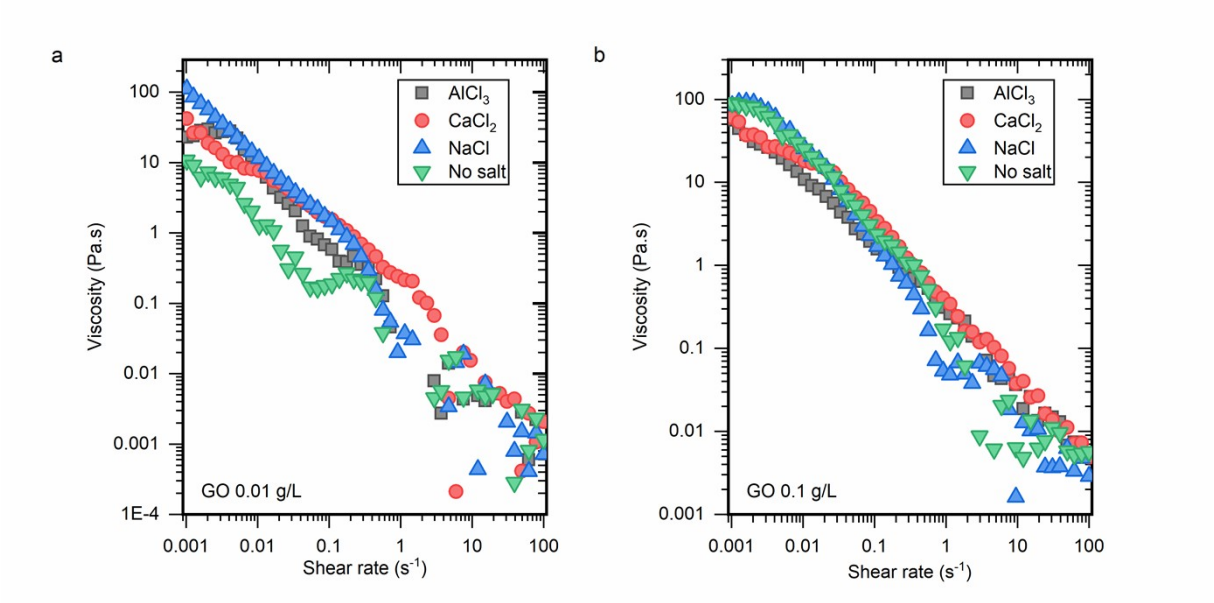

Fig. S8. Shear viscosity of dilute graphene oxide dispersions as a function of shear rate at different salts concentrations is depicted in for graphene oxide concentration of a) 0.01 g/L and b) 0.1 g/L.

References:

1 Chowdhury, I., Duch, M. C., Mansukhani, N. D., Hersam, M. C. & Bouchard, D. Colloidal Properties and Stability of Graphene Oxide Nanomaterials in the Aquatic Environment. *Environ. Sci. Tech.* **47**, 6288-6296 (2013).

2 Wu, L. *et al.* Aggregation Kinetics of Graphene Oxides in Aqueous Solutions: Experiments, Mechanisms, and Modeling. *Langmuir* **29**, 15174-15181 (2013).

3 Yang, K., Chen, B., Zhu, X. & Xing, B. Aggregation, Adsorption, and Morphological Transformation of Graphene Oxide in Aqueous Solutions Containing Different Metal Cations. *Environ. Sci. Tech.* **50**, 11066-11075 (2016).

4 Tang, H. *et al.* New Insight into the Aggregation of Graphene Oxide Using Molecular Dynamics Simulations and Extended Derjaguin–Landau–Verwey–Overbeek Theory. *Environ. Sci. Tech.* **51**, 9674-9682 (2017).

5 Sun, B., Zhang, Y., Chen, W., Wang, K. & Zhu, L. Concentration Dependent Effects of Bovine Serum Albumin on Graphene Oxide Colloidal Stability in Aquatic Environment. *Environ. Sci. Tech.* **52**, 7212-7219 (2018).

6 Gao, Y. *et al.* Exploring the Aggregation Mechanism of Graphene Oxide in the Presence of Radioactive Elements: Experimental and Theoretical Studies. *Environ. Sci. Tech.* **52**, 12208-12215 (2018).

7 Gao, Y. *et al.* Insights into key factors controlling GO stability in natural surface waters. *J. Hazard. Mater.* **335**, 56-65 (2017).

8 Wang, D. *et al.* How and Why Nanoparticle's Curvature Regulates the Apparent pKa of the Coating Ligands. *J. Am. Chem. Soc.* **133**, 2192-2197 (2011).

9 Dreier, L. B. *et al.* Saturation of charge-induced water alignment at model membrane surfaces. *Sci. Adv.* **4**, eaap7415 (2018).

10 Manning, G. S. The Interaction between a Charged Wall and Its Counterions: A Condensation Theory. *J. Phys. Chem. B* **114**, 5435-5440 (2010).

11 Brown, M. A., Goel, A. & Abbas, Z. Effect of Electrolyte Concentration on the Stern Layer Thickness at a Charged Interface. *Angew. Chem. Int. Ed.* **55**, 3790-3794 (2016).

12 Siretanu, I. *et al.* Direct observation of ionic structure at solid-liquid interfaces: a deep look into the Stern Layer. *Sci. Rep.* **4**, 4956 (2014).

13 Brown, M. A. *et al.* Determination of Surface Potential and Electrical Double-Layer Structure at the Aqueous Electrolyte-Nanoparticle Interface. *Phys. Rev. X* **6**, 011007 (2016).

14 Trefalt, G., Behrens, S. H. & Borkovec, M. Charge regulation in the electrical double layer: ion adsorption and surface interactions. *Langmuir* **32**, 380-400 (2016).

15 in *Intermolecular and Surface Forces (Third Edition)* (ed Jacob N. Israelachvili) iii (Academic Press, 2011).

16 Moazzami-Gudarzi, M. *et al.* Interactions between similar and dissimilar charged interfaces in the presence of multivalent anions. *Phys. Chem. Chem. Phys.* **20**, 9436-9448 (2018).

17 Trefalt, G., Szilagyi, I. & Borkovec, M. Poisson–Boltzmann description of interaction forces and aggregation rates involving charged colloidal particles in asymmetric electrolytes. *J. Colloid Interface Sci.* **406**, 111-120 (2013).

18 Gudarzi, M. M. Colloidal Stability of Graphene Oxide: Aggregation in Two Dimensions. *Langmuir* **32**, 5058-5068 (2016).

19 Weiss, M. *et al.* Density of surface charge is a more predictive factor of the toxicity of cationic carbon nanoparticles than zeta potential. *J. Nanobiotech.* **19**, 5 (2021).

20 Poulin, P. *et al.* Superflexibility of graphene oxide. *Proc. Natl. Acad. Sci. U. S. A.* **113**, 11088-11093 (2016).

21 Helfrich, W. Effect of thermal undulations on the rigidity of fluid membranes and interfaces. *J. Phys. France* **46**, 1263-1268 (1985).